








Article

Study on the Impact of a Combination of Synthetic Wollastonite and 2-Mercaptobenzothiazole-Based Fillers on UHMWPE Polymeric Matrix

Sakhayana N. Danilova ^{1,*}, Aitalina A. Okhlopkova ¹, Sofia B. Yarusova ^{2,3}, Afanasy A. Dyakonov ¹, Pavel S. Gordienko ², Evgeniy K. Papynov ⁴, Oleg O. Shichalin ⁴, Igor Yu. Buravlev ⁴, Andrey P. Vasilev ¹, Ivan G. Zhevtun ² and Natalya V. Ivanenko ⁵

- ¹ Chemical Department, Institute of Natural Sciences, North-Eastern Federal University, Yakutsk 677000, Russia; okhlopkova@yandex.ru (A.A.O.); afonya71185@mail.ru (A.A.D.); gtvap@mail.ru (A.P.V.)
- ² Institute of Chemistry, Far Eastern Branch, Russian Academy of Sciences, Vladivostok 690022, Russia; yarusova_10@mail.ru (S.B.Y.); gordienko@mail.ru (P.S.G.); jevtun_ivan@mail.ru (I.G.Z.)
- ³ Department of Ecology and Environmental Problems of Chemical Technology, Vladivostok State University, Vladivostok 690014, Russia
- ⁴ Department of Nuclear Technology, Far Eastern Federal University, Vladivostok 690922, Russia; papynov@mail.ru (E.K.P.); oleg_shich@mail.ru (O.O.S.); buravlev.i@gmail.com (I.Y.B.)
- ⁵ Department of Ecology, Biology and Geography, Vladivostok State University, Vladivostok 690014, Russia; natalya.ivanenko@vvsu.ru
- * Correspondence: dsn.sakhayana@mail.ru

Abstract: This study investigates the impact of a binary filler on the physicochemical and tribological properties, as well as structure, of polymeric composite materials based on ultra-high-molecular-weight polyethylene. The organic modifier—2-mercaptobenzothiazole and wollastonite particles synthesized from two different systems (modeled and derived from waste) were used as the binary filler. The synthesis of wollastonite was carried out in the complex model system ($\text{CaSO}_4 \cdot 2\text{H}_2\text{O} - \text{SiO}_2 \cdot n\text{H}_2\text{O} - \text{KOH} - \text{H}_2\text{O}$) and from technogenic waste (borogypsum). It was demonstrated that the introduction of the binary filler made it possible to obtain an optimal combination of mechanical and tribological properties. It was found that during the wear of polymeric composite materials loaded with organic fillers, the fillers migrate to the friction surface, providing a shield against abrasive wear of the steel counterface. Due to the modification of ultra-high-molecular-weight polyethylene by 2-mercaptobenzothiazole, the interdiffusion of polymeric matrix macromolecules and interphase coupling with wollastonite particles improve. The 2-mercaptobenzothiazole organic compound used as the filler facilitates the relaxation processes within the composite under external loads.

Keywords: polymer composite materials; ultra-high molecular weight polyethylene; wollastonite; 2-mercaptobenzothiazole



Citation: Danilova, S.N.; Okhlopkova, A.A.; Yarusova, S.B.; Dyakonov, A.A.; Gordienko, P.S.; Papynov, E.K.; Shichalin, O.O.; Buravlev, I.Y.; Vasilev, A.P.; Zhevtun, I.G.; et al. Study on the Impact of a Combination of Synthetic Wollastonite and 2-Mercaptobenzothiazole-Based Fillers on UHMWPE Polymeric Matrix. *J. Compos. Sci.* **2023**, *7*, 431. <https://doi.org/10.3390/jcs7100431>

Academic Editor: Aleksey A. Vedyagin

Received: 20 September 2023

Revised: 8 October 2023

Accepted: 11 October 2023

Published: 13 October 2023



Copyright: © 2023 by the authors. Licensee MDPI, Basel, Switzerland. This article is an open access article distributed under the terms and conditions of the Creative Commons Attribution (CC BY) license (<https://creativecommons.org/licenses/by/4.0/>).

1. Introduction

Construction materials based on polymeric composite materials (PCMs) ensure the reliability and durability of friction units and a reduction in the cost of the operation and repair of vehicles. At the same time, they can be easily converted into complex-shaped products, which simplifies the manufacturing process [1,2].

One of the promising matrices for manufacturing such materials is ultra-high-molecular-weight polyethylene (UHMWPE), which, in recent years, has been introduced into various industries due to its unique properties [3]. UHMWPE possesses high strength and chemical resistance, sufficient wear resistance, and a low friction coefficient [4–6]. Moreover, a wide range of operational properties of UHMWPE composite materials can be achieved by adding different fillers [7,8] and using different technological methods for matrix modification: ultrasonic processing [9,10], radiation modification [11,12], and mechanical stimulus in

a planetary mill [13,14]. However, in most cases, these methods do not lead to a significant improvement in the complex of mechanical and tribological properties.

Currently, the use of an optimal combination of fillers of various natures and geometries in a polymeric matrix makes it possible to sufficiently improve the operational characteristics of PCMs due to their synergetic effect [15]. In this study, wollastonite, in combination with the organic component—2-mercaptobenzothiazole (MBT), was used as a binary modifier of UHMWPE.

The choice of wollastonite is based on its reinforcing action on the polymer matrix. In this paper, we propose using wollastonite with a needle-like particulate habitus synthesized via the hydrothermal method as a nanofiller. The advantage of using synthetic wollastonite stems from the possibility of varying the size and shape of its particles. Various low-temperature or high-temperature methods involving subsequent thermal treatment of intermediate compounds or direct solid-phase reactions are used to synthesize wollastonite and accompanying intermediates, including calcium hydrosilicates [16–18]. Depending on the method, synthesis conditions, and initial reagents, the formation of wollastonite particles of differing morphology is observed. The use of wollastonite as a filler for UHMWPE was considered in the following works [19–22], where a significant increase in material strength and wear resistance was achieved. However, there is a challenge of coupling with a polymeric matrix due to weak interphase interaction. This is because the nature of the interaction between a filler and polymeric matrix in the composites, which are heterogeneous multicomponent systems, is complex. Weak adhesion strength and the absence of interphasic interaction between components may lead to defects in the composite structure, which negatively affects the physicomachanical and tribotechnical properties of the material. One promising method to improve interphase interaction is chemical and technological modification, which involves modifying the polymer with substances of high reactivity. To improve the dispersion of wollastonite particles in the polymer volume and its interphasic interaction, an organic modifier MBT was used, which is a reactive compound. There are studies in which organic fillers (wood flour, bamboo filament, polymers, cellulose, vitamin E, paraffin, etc.) were used for UHMWPE modification [23–26]. Currently, the usage of MBT as a modifier of UHMWPE is not fully explored, particularly as an adhesion promoter in PCMs.

The aim of this study is to investigate the influence of binary fillers of different natures on the mechanical and tribological properties and structure of UHMWPE.

2. Materials and Methods

2.1. Study Objects

UHMWPE of the GUR-4022 brand (Celanese, Nanjing, China) with a molecular weight of 5 million g/mol was used as a polymeric base. MBT (GOST 739-74) and synthesized wollastonite particles were used as fillers [27]. Wollastonite was synthesized by autoclaving in a model system (MW) and from borogypsum (WB):

1. The precursor components in the model system were calcium sulfate $\text{CaSO}_4 \cdot 2\text{H}_2\text{O}$ (p.a.), silicon dioxide (pur.), and potassium hydrate (p.a.), which were mixed in a stoichiometric ratio.
2. In the second case, borogypsum was processed in an autoclave by a potassium hydrate solution (p.a.) in a stoichiometric ratio. The base components of borogypsum were calcium sulfate dihydrate and amorphous silica.

Synthesis of wollastonite was carried out in an autoclave at 220 °C for 3 h. After the designated time interval, the obtained precipitate mixture was removed from the autoclave, flushed out by distilled water heated up to 60–70 °C, separated from the solution by filtration through the Blue ribbon filter paper, and dehydrated at 85 °C for several hours. The resulting precipitates were further calcined in a TSNOL 6.7/1300 muffle furnace (SNOL, Lithuania) in a temperature range of 900–1000 °C for 1–3 h.

2.2. PCM Fabrication Technology

The initial UHMWPE powder was primarily dehydrated in a PE-0041 furnace (Ecopribor, Saint Petersburg, Russia) for 1.5 h to remove the adsorbed moisture. Before use, wollastonite was dehydrated at 85 °C for 4 h. The fillers for UHMWPE were used both separately and in combination (Table 1).

Table 1. Composition of the PCM and the content of fillers, wt.%.

Composite	UHMWPE	MBT	Wollastonite
1	99	0.5	0.5
2	98.5	0.5	1
3	97.5	0.5	2
4	94.5	0.5	5
5	98.5	1	0.5
6	98	1	1
8	97	1	2
9	94	1	5

UHMWPE and the fillers were mixed at room temperature in a paddle mixer with a rotor speed of 1200 rpm. Processing of UHMWPE and the composite materials was performed using a hot-pressing process using a PCMV-100 hydraulic press (Impuls, Moscow, Russia) at a temperature of 175 °C, a pressure of 10 MPa, and a curing time of 20 min, followed by cooling under pressure to room temperature.

2.3. Research Methods

The stress–strain properties of the PCM were determined using an AGS-J universal breaking machine (Shimadzu, Tokyo, Japan). The studies were conducted in accordance with ASTM D3039/D3039M-14 standards [28]. The speed of moving grips was 50 mm/min, and the number of parallel tests per PCM series was 6.

The tribological characteristics of UHMWPE and the PCM were defined on a UMT-3 testing machine (CETR, Mountain View, CA, USA) at a specific load of 1.9 MPa and a linear sliding speed of 0.5 m/s under the “finger-disk” friction scheme over 3 h. The samples with a diameter of 10 mm and a height of 20 mm were used for the studies. The disks made of AISI 1045 steel characterized by a strength of 45–50 HRC and a roughness of $R_a = 0.06\text{--}0.08\ \mu\text{m}$ were used as the counterface. Each result of the tribotechnical tests is presented as the arithmetical average of 3 measurements.

The accumulation time at the point was 0.2 s. SEM images of samples’ surfaces were obtained using a Carl Zeiss Ultra 55 scanning electron microscope (SEM, Oberkochen, Germany), with the prefix for energy-dispersive X-ray microanalysis (EDX) Bruker (GmbH, Berlin, Germany).

The IR spectra of MBT and the surfaces of the samples before and after friction were recorded using a Varian 7000 FT-IR Fourier transform IR spectrometer (FTIR; Varian 7000, Palo Alto, CA, USA) with an attenuated total internal reflection set in the wavenumber range of $4000\text{--}400\ \text{cm}^{-1}$.

The specific surface of the synthesized wollastonite particles was studied by a NOVA Autosorb IQ low-temperature adsorption machine (Quantachrome Instruments, Boynton Beach, FL, USA).

The X-ray diffraction (XRD) patterns of wollastonite were recorded using a D8 ADVANCE automatic diffractometer (Bruker, Karlsruhe, Germany) with sample rotation in $\text{CuK}\alpha$ -radiation. XRD analysis was carried out using the EVA search–match software with the Powder Diffraction File TM database (Soorya N Kabekkodu, 2007). The X-ray patterns of the PCM were obtained using an ARL X’Tra X-ray powder diffractometer (Thermo Fisher Scientific, Zug, Switzerland). An X-ray tube with a copper anode ($\lambda(\text{CuK}\alpha) = 0.154\ \text{nm}$) was used as a radiation source. The scanning angles were from 3° to 60° with a scan step of 0.05° and an acquisition interval of 3 secs at each point in the reflection mode.

3. Results

3.1. Study of the Synthesized Wollastonite Particles

The results of the XRD analysis and the morphology of the synthesized wollastonite particles based on the initial components are presented in Figure 1.

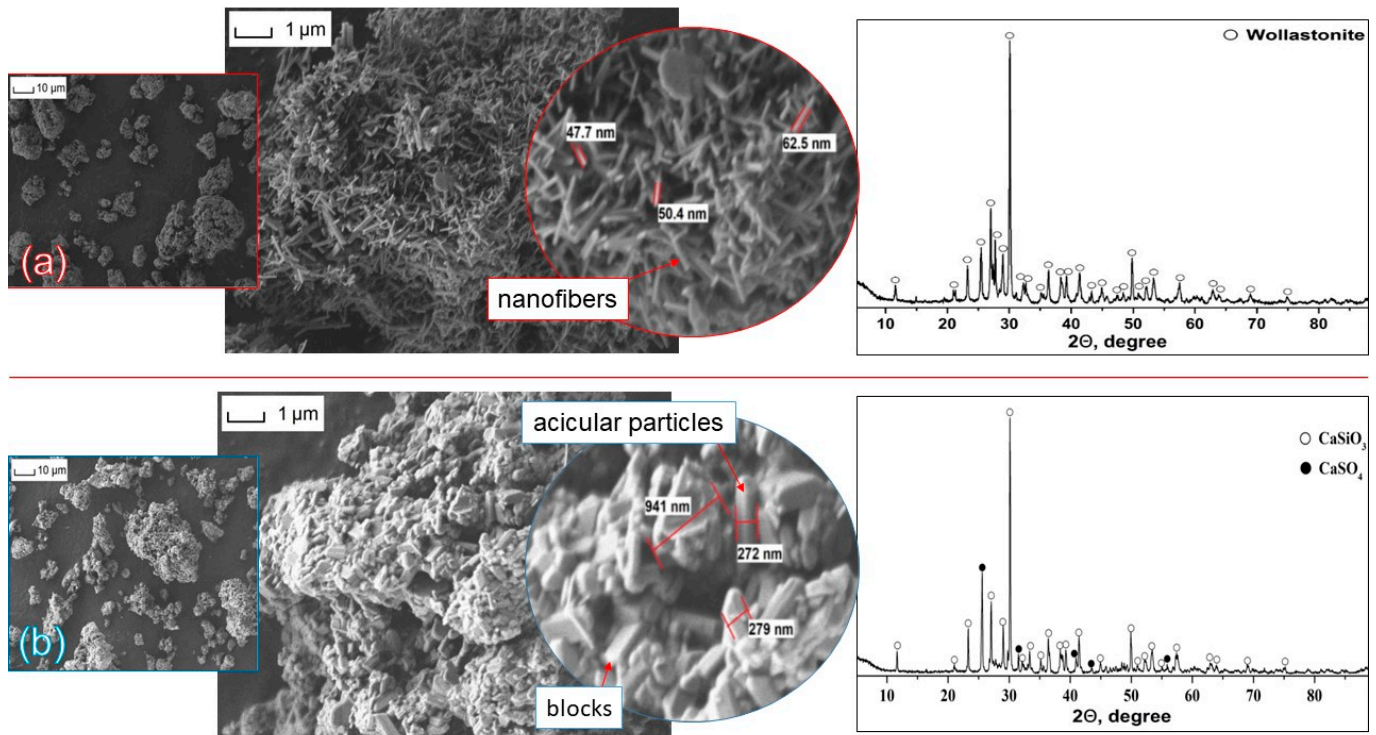


Figure 1. The morphology and the X-ray diffraction pattern of the synthesized wollastonite particles: (a)—model wollastonite MW, (b)—wollastonite from borogypsum WB.

Figure 1 shows that the synthesized wollastonite is characterized by the formation of agglomerates, but the form and size of particles differ depending on the initial components. For instance, the agglomerates from model wollastonite consist of nanofibers with a diameter of ~ 47.7 – 62.5 nm and a specific surface of 26.4 m²/g. It is evident that the agglomerate of borogypsum wollastonite consists of acicular particles and blocks with delineated planes, including fine-grained nanosized particles. In this case, the diameter of the aciculae is up to 280 nm, and the size of large particles is 940 nm. The specific surface area of wollastonite particles synthesized from borogypsum after annealing equals 0.82 m²/g. The size dispersion of wollastonite particles synthesized from borogypsum and its model counterpart may be attributed to the presence of microimpurities in the composition of technogenic waste, which influence the growth kinetics and morphology of wollastonite particles.

The analysis of the XRD pattern of wollastonite shows that triclinic CaSiO₃ is formed in a model system (PDF-2, 01-084-0654: $a = 7.92580$; $b = 7.32020$; $c = 7.06530$; $\alpha = 90.055$; $\beta = 95.217$; $\gamma = 103.426$), and the sample from borogypsum is characterized by the presence of monoclinic CaSiO₃ wollastonite (PDF-2, 00-027-0088: $a = 15.36000$; $b = 7.28500$; $c = 7.08400$; $\alpha = 90.000$; $\beta = 95.400$; $\gamma = 90.000$) and unreacted calcium sulfate CaSO₄ (PDF-2, 01-072-2297: $a = 6.23000$; $b = 6.98000$; $c = 6.97000$; $\alpha = 90.000$; $\beta = 90.000$; $\gamma = 90.000$).

The particle size distribution of wollastonite is exhibited in Figure 2.

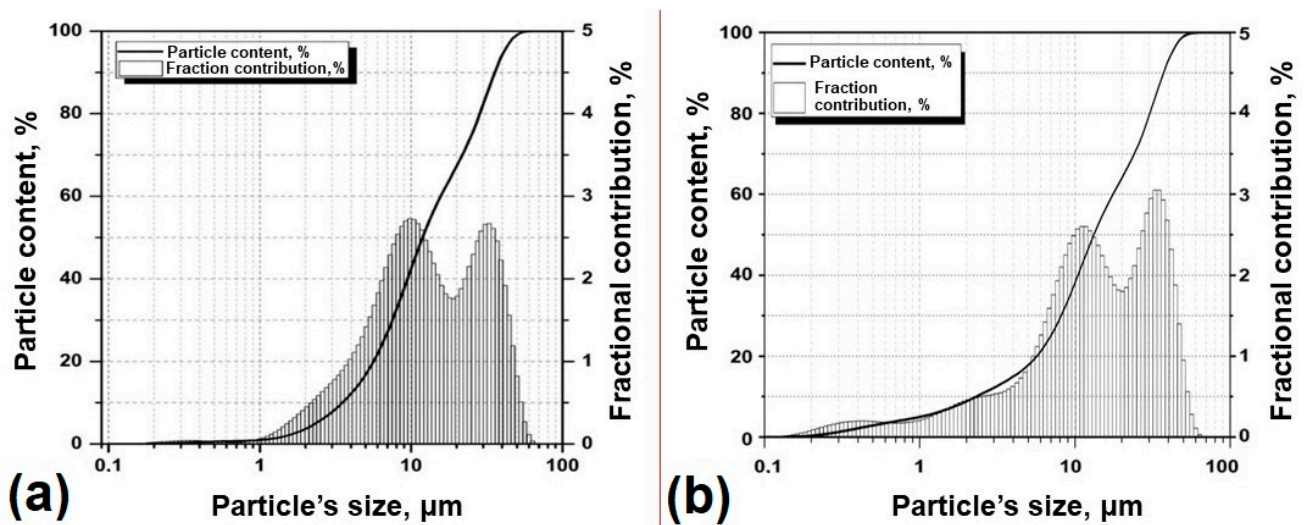
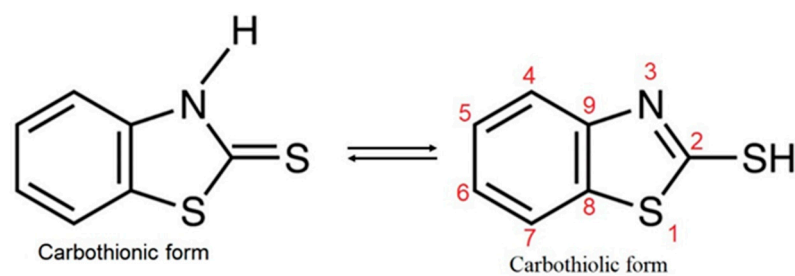


Figure 2. The size distribution of wollastonite particles: (a)—model wollastonite MW, (b)—wollastonite from borogypsum WB.

The analysis of the particle size distribution of MW indicates that the particles are characterized by the formation of agglomerates with sizes ranging from 9–11 to 30–40 microns. Whereas the results of particle size distribution of WB revealed that the sizes of wollastonite agglomerates vary from 0.2 to 70 μm (Figure 2b).

3.2. Characterization of MBT

2-Mercaptobenzothiazole $\text{C}_7\text{H}_5\text{NS}$ is an organic compound of the benzothiazole class with a melting point of 179 $^\circ\text{C}$. It exists as the carbothionic and carbothiolic tautomer (Scheme 1). In a study [29], crystal structure analysis revealed that the carbothionic form predominates in MBT. In another study [30] demonstrated using the Hartree–Fock method and DFT that the carbothionic form was more stable than the carbothiolic one by 39–44 kJ/mol. Furthermore, it was proven [29] that MBT formed asymmetric dimers through $\text{N H}\cdots\text{S}$ hydrogen bonds. It was also shown that the dimeric form of MBT, connected through hydrogen bonds, is more stable compared to its tautomeric monomers.



Scheme 1. The carbothionic and carbothiolic tautomer of the MBT.

The $-\text{SH}$ mercapto group is characterized by proton-donor activity and is classified among weak Lewis acids and Pearson soft bases [31]. The heterocycle provides stability to transition compounds through the formation of a conjugated electron system, i.e., the delocalization of electron density [32].

Based on the chemical character, MBT is used in lubricating oils as an antiwear additive and is used in the industry as a copper corrosion inhibitor and as a collector in flotation [33–35]. Moreover, MBT is widely used in the rubber industry as a vulcanizing accelerator and a curing agent [36–38].

The structure and properties of MBT are extensively studied in the following works [29,39–45]. For the reliability of the used MBT, IR spectroscopy and SEM stud-

ies were performed, the results of which are presented in Figure 3. The microphotograph shows that MBT is characterized by a wide range of particle sizes and forms. The friable and porous surface is observed on scaling.

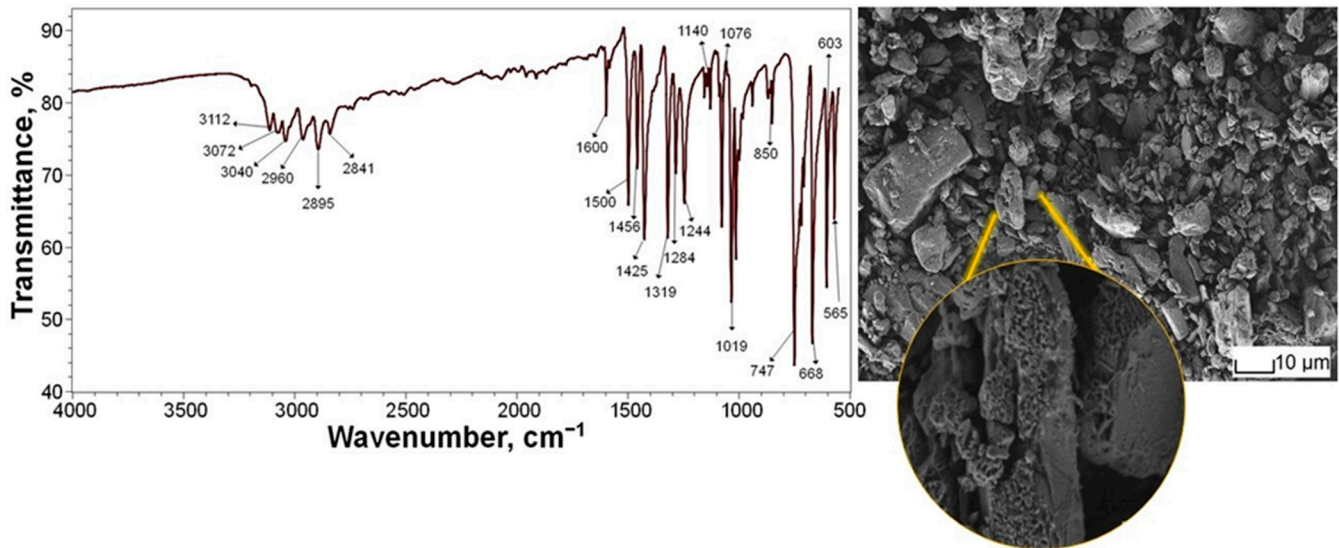


Figure 3. The IR spectrum and the morphology of MBT.

The bands at 3112, 3072, 3040, 2960, 2895, and 2841 cm^{-1} are observed in the high wavenumber region of the IR spectrum of the initial MBT. The bands correspond to the asymmetric and symmetric stretching modes of the C–H bond. The presence of intensive absorption bands in the region of 1600–560 cm^{-1} is found. For example, peaks at 1600, 1500, and 1076 cm^{-1} correspond to the C–C bond of the aromatic cycle. Maxima at 1456, 1319, and 1140 cm^{-1} correspond to the in-plane C–H vibration of the methyl group. The vibration motions of the C–H bond produce 850 and 747 cm^{-1} peaks. The maximum at 1425 cm^{-1} corresponds to in-plane deformation vibrations of the N–H bond, and the peak at 565 cm^{-1} is caused by the vibration of this bond. Moreover, the recorded maxima at 1284 and 1244 cm^{-1} correspond to symmetric and asymmetric vibrations of the C–N bond. The presence of the mercapto group can be defined by the intensive peak at 1019 cm^{-1} , which corresponds to the S=C bond vibration of the MBT carbothionic form. The maximum at 668 cm^{-1} can be attributed to the S–C bond vibration and to the bending vibration of the C–C–C bond; the latter may induce the maxima at 603 cm^{-1} . Therefore, the detected bands in the IR spectra correspond to the molecule structure of the initial MBT [30,44,46].

3.3. Stress–Strain Properties of the PCM

To investigate the effect of the MBT reactive filler on the interphase interaction of UHMWPE and wollastonite (MW and WB), studies of the stress–strain properties of the PCM were conducted, and the results are presented in Figure 4. The stress–strain curve of the composites is shown in Figure 5. The values with a single content of each filler in the PCM are presented for comparison.

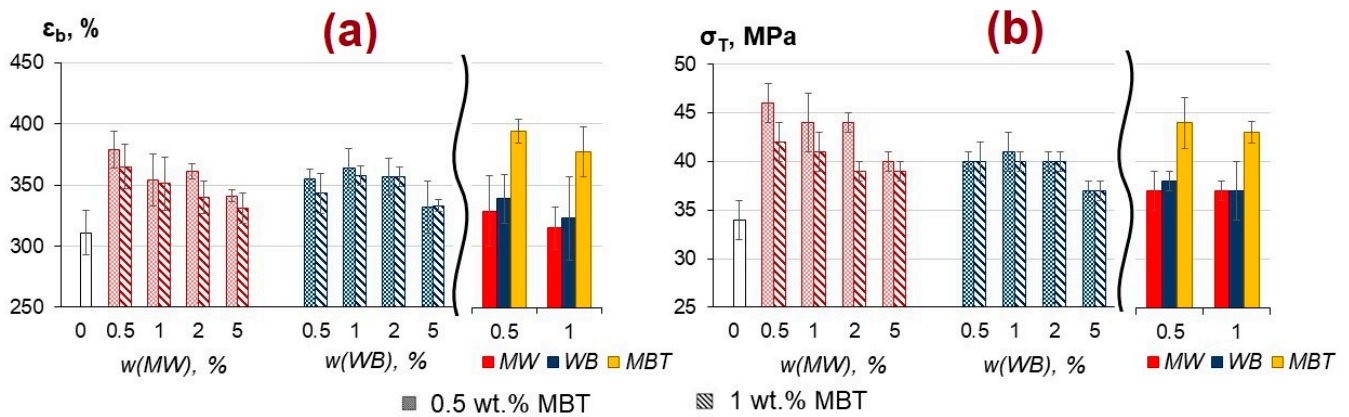


Figure 4. Stress–strain properties of UHMWPE and the PCM: (a) ϵ_b —total extension at fracture, %; (b) σ_T —tensile strength, MPa.

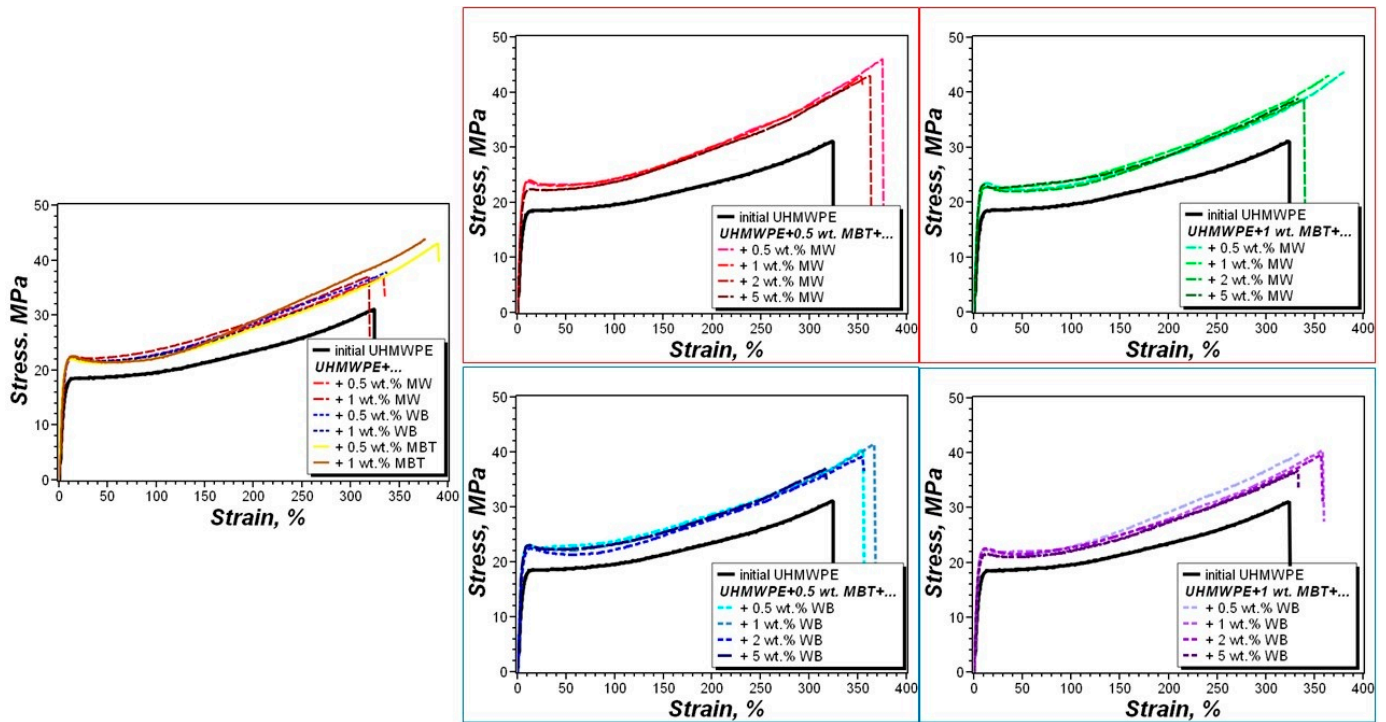


Figure 5. Stress–strain curve of the tensile tests.

It was found that the introduction of a filler, consisting of the “MBT—model wollastonite”, into UHMWPE contributed to the maximum increase in tensile strength compared to other composites (ratio 1 wt.% MW and 0.5 wt.% MBT). An increase in total extension at fracture by 22% and tensile strength by 35% compared to the initial UHMWPE was observed. It was established that the usage of the “MBT-wollastonite from borogypsum” system led to a 21% increase in tensile strength and a negligible increase in the total extension coefficient of the PCM by 17%. The composites, loaded with single fillers, were characterized by some increase in tensile strength, while the value of total extension at fracture was similar to the initial UHMWPE. A notable difference is observed in the composite filled with MBT, where an increase in tensile strength by 29% and relative elongation at break by 27% compared to UHMWPE are recorded.

One of the factors in obtaining high-strength composite materials is reinforcing the adhesive interaction between the composite components and forming interphase layers possessing properties that differ from those of the polymer. The increase in the stress–strain

characteristics when introducing the binary filler can be attributed to the reinforcement of the interaction between the composite components due to the reactivity of MBT. Thereby, wollastonite fully implements a reinforcing function in the matrix, taking into account the size and form of wollastonite particles. Since synthesized MW has a more homogeneous nanofiber structure, the “MBT-model wollastonite” system of modifiers proves to be the most effective.

3.4. Study of the Structure of UHMWPE and the PCM

Studies of the supramolecular structure of the initial UHMWPE and the PCM, modified by 1 wt.% of each filler, were performed in Figure 6.

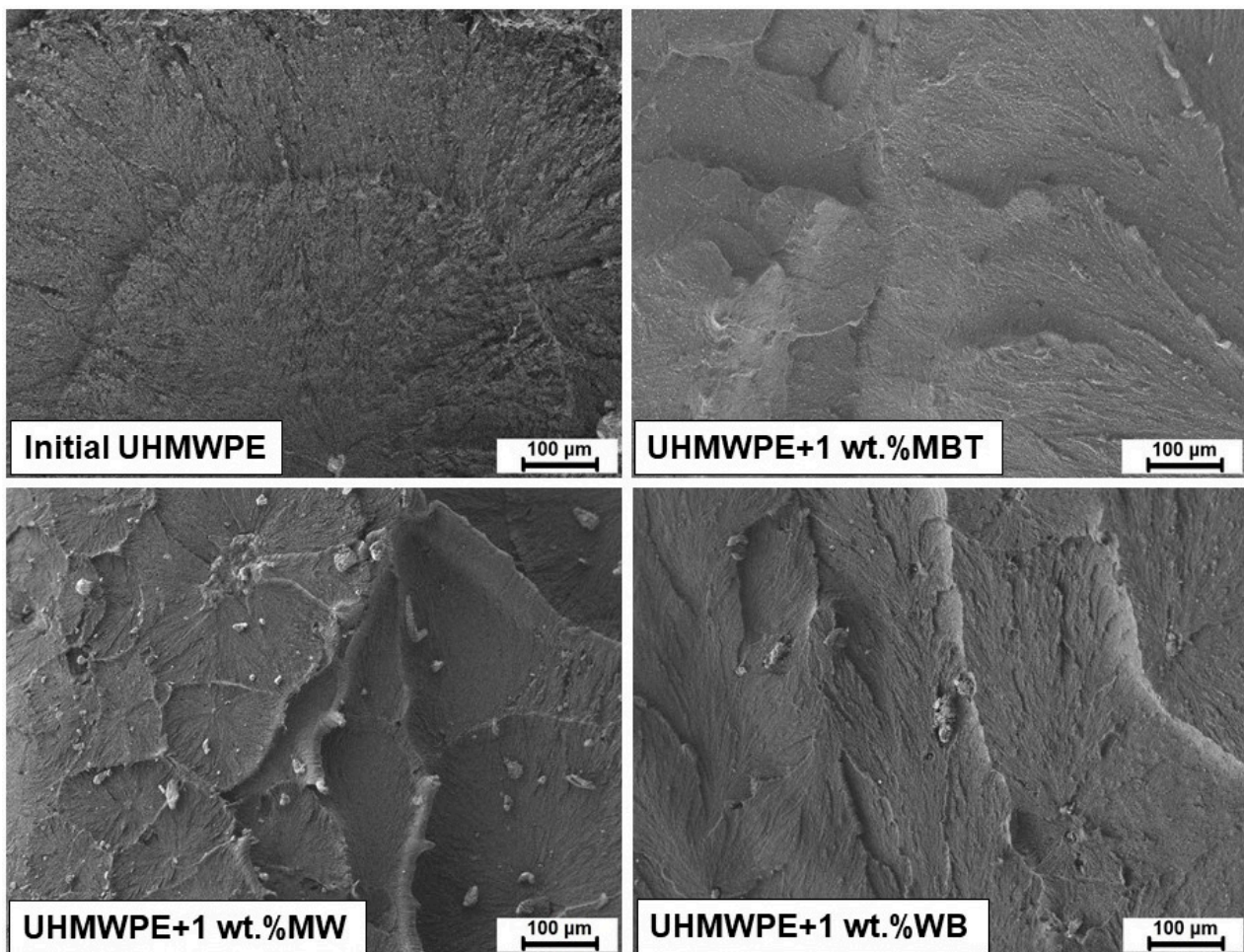


Figure 6. The microphotograph of the supramolecular structure of the initial UHMWPE and the composites comprising single fillers (scale X150).

A large-sized spherulite structure with a loose packing of fibrils is observed in the microphotograph of the initial UHMWPE. The formation of small-sized radial spherulite-like structures with varying-sized structure elements is observed with wollastonite introduced in the PCM. Wollastonite particles are artificial nucleating agents that contribute to the formation of a more ordered and oriented structure throughout the section. In the case of MBT introduction, the formation of an inhomogeneous structure is observed. Moreover, filler particles are uniformly distributed throughout UHMWPE, and the presence of agglomerated filler particles is not observed.

Figures 7–10 show the microphotographs of the supramolecular structure of the PCM modified by the binary filler.

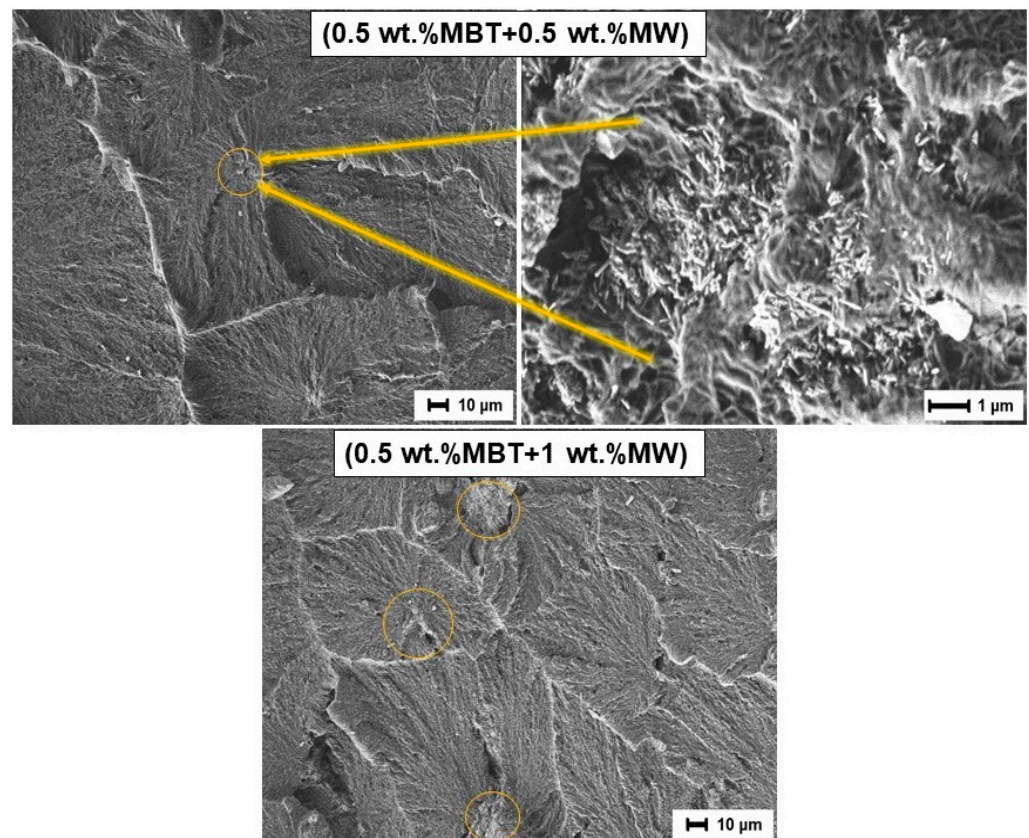


Figure 7. Supramolecular structure of the PCM based on the ratio of fillers (scale X500 and X1000).

From the microphotographs of PCM (Figures 7 and 8), it was established that small-sized spherulite-like formations appeared in the structure of the PCM in the case of the simultaneous presence of wollastonite and MBT, whereas it was not observed in the case of pure MBT. It is related to the fact that the organic filler disperses agglomerated particles of the MW in the polymer, which is confirmed by the absence of agglomerates (Figure 6). Thus, it is shown that the introduction of the MBT organic filler leads to the activation of wollastonite particles during UHMWPE crystallization. Additionally, it is evident that this tendency increases with an increase in the content of nanoparticles, i.e., the number of MB particles as crystallizing nuclei become larger (Figure 6).

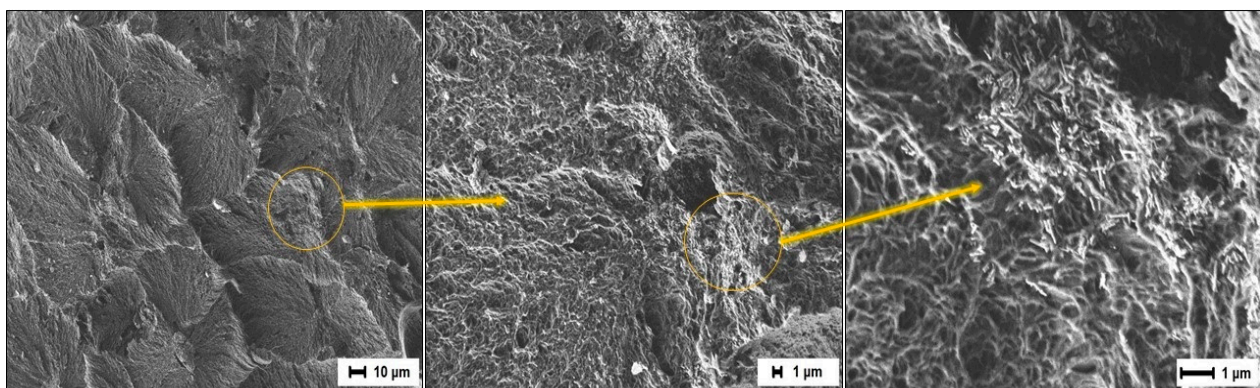


Figure 8. Supramolecular structure of the PCM, containing 1 wt.% MBT and 0.5 wt.% at different scales: X500 → X3000 → X10,000.

A rise in UHMWPE crystallization with the formation of well-defined spherulites is observed with an increase in MBT content. Figure 8 shows that the migration of MW

nanoparticles to the boundaries of spherulites is also observed. One can assume that the mobility of nanofibers in the polymer rises with an increase in the MBT content, and the filling of regions with lower surface energy occurs (zones where spherulites overlap).

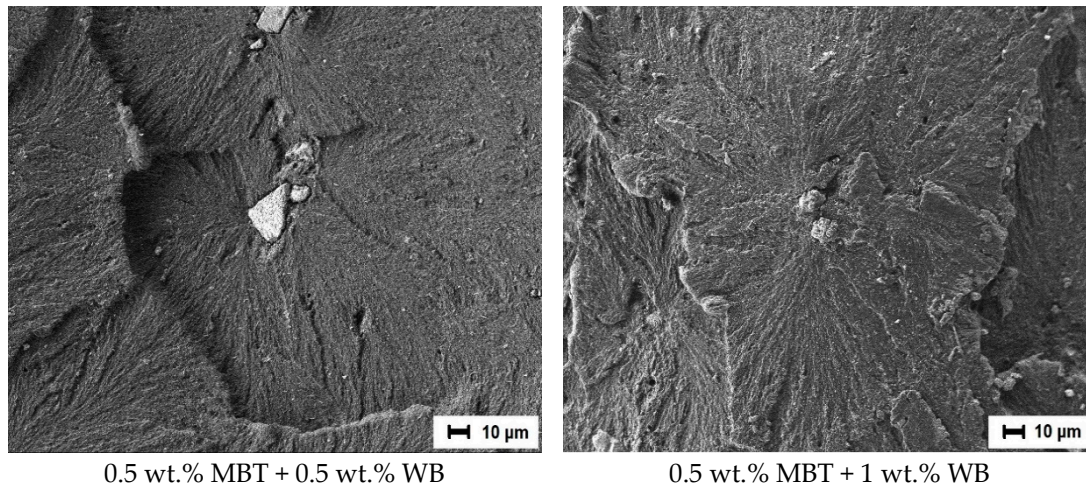


Figure 9. Supramolecular structure of the PCM with a binary modifier.

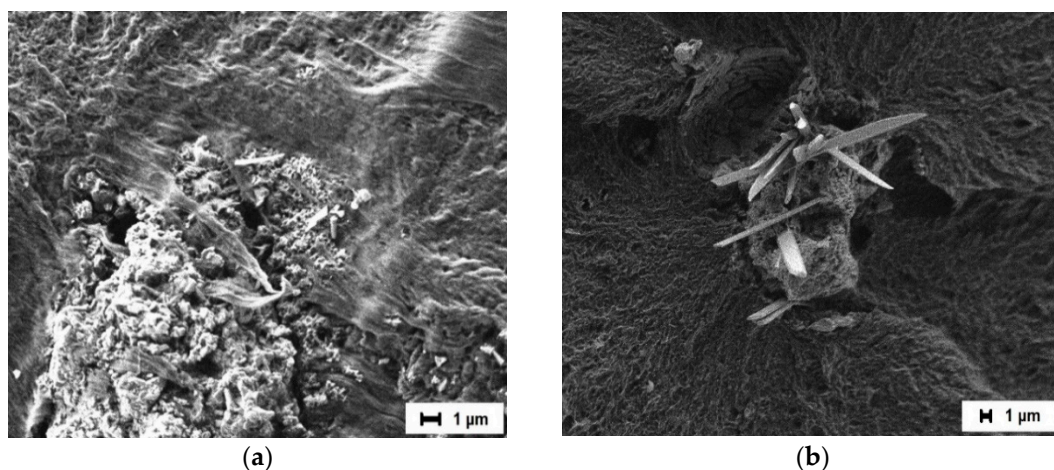


Figure 10. The microphotograph of the PCM, containing 1 wt.% MBT and 1 wt.% WB, scale (a)—X5000 and (b)—X3000.

The structural homogeneity of the material is achieved when filler particles are well dispersed in the polymer. In this case, local strains are reduced, which has a positive effect on the relaxation processes. The issue of the dispersion of agglomerated nanoparticles in UHMWPE was addressed in the work [47], where a developed technology of combining PCM components under ultrasonic vibrations in a liquid medium (in ethanol) is described. The composition materials using this method are characterized by a significant improvement in wear resistance and deformation-strength properties. In addition, one of the common ways of dispersing fillers is the use of mechanical activation in a planetary mill, which is due to the simplicity and universality of the method [48–51]. Also, there are alternative ways of dispersing agglomerates using laser treatment [52] and additional modification of nanoparticles by adhesion promoters and surfactants [20,53–55]. These methods include a supplement of additional stages in the composite production, which in turn complicates the process. In a series of works [56–58], the influence of binary filler with paraffin and carbon nanotubes on the properties of UHMWPE is demonstrated. The authors proved that paraffin oil improved the filler dispersion in the polymer and the interdiffusion of UHMWPE globules. Based on this idea, MBT can be adsorbed on the

wollastonite surface, which increases the mobility of macromolecules in the matrix volume (acting as a plasticizer). However, the mechanism of action may differ as MBT can spontaneously form an adsorption monolayer on the wollastonite surface, thereby reinforcing interphase interaction and increasing the wettability of the particles with the binder, which additionally orients them in volume. In addition, stable free radicals may appear from the MBT particle, which initiates the processes of supramolecule structuring.

In the case of wollastonite from borogypsum with MBT, the formation of a nontypical supramolecular structure was observed in UHMWPE. Figure 1 shows that wollastonite particles from borogypsum have various forms. The particles with layered and sponge-like structures (micron size) become a crystallization center of the spherulites, and small acicular particles are distributed throughout the volume, as seen in the microphotographs of the PCM with a binary filler (Figure 9). It is seen that the spherulite sizes are smaller compared to the composites loaded only with WB (Figure 4); however, they are larger compared to the binary filler with model wollastonite.

It was defined that MBT covered the surface of layered particles, whereas in the case of spongy wollastonite particles, the interphase coupling with the polymer improved (Figure 10). It is seen that the polymer fibrils partially cover the surface of MB particles and penetrate the space between the agglomerates.

It was found that the increase in WB (from 1 wt.%) led to the agglomeration of acicular particles of the filler. In the case of agglomerates of acicular particles, MBT filled the interphase layer between the filler and the polymer. The localization of MBT on the interphase border is called the Pickering effect when the interphase surface tension is decreased [59–62]. The MBT particles in the interfacial layer can act as additional “molecular clamps” according to a figurative expression [63], which explains the changes in the material’s mechanical behavior. In this case, MBT particles play a role as a compatibilizer between wollastonite and UHMWPE [64]. Thus, the increase in the stress–strain properties of the PCM is explained by the dispersion of wollastonite particles due to the chemical nature of MBT, as well as the improvement of interphase interaction caused by the reactivity of the MBT.

The influence of wollastonite particles depending on the filler content on the crystalline state of UHMWPE was studied by XRD. The X-ray patterns of UHMWPE and the PCM are shown in Figure 11.

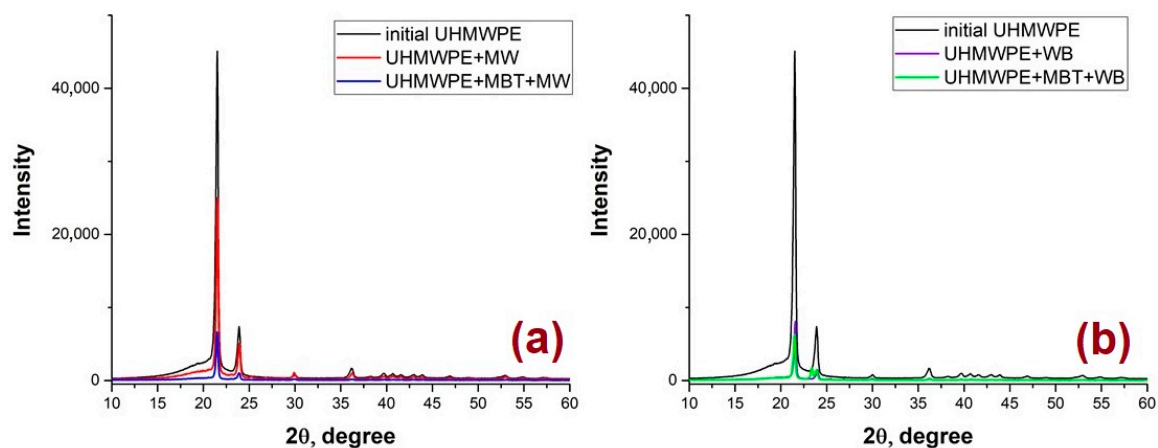


Figure 11. X-ray diffraction patterns of UHMWPE and the PCM, containing 1 wt.% and 5 wt.% wollastonite: (a)—model and (b)—from borogypsum.

The X-ray patterns of UHMWPE and the PCM reveal two main reflexes (2θ — 21.4° and 23.9°) corresponding to two 200 and 110 planes of the UHMWPE crystal phase in the orthorhombic cell. The other reflexes at 2θ in the region of 30 – 60° of the UHMWPE crystal phase are relatively weak and will not be considered in further analysis of the UHMWPE structure. A region around $2\theta \sim 19.3^\circ$ corresponds to an amorphous ring (010) [65]. The

decrease in the amorphous ring and some decline in the crystalline peaks compared to the initial UHMWPE are observed with MW introduction. It indicates the enlargement of a number of the crystallizing centers (nucleation) in UHMWPE during the formation of the crystal structure. It is established that MW affects the amorphous regions of a polymeric matrix and decreases the defectiveness of the PCM crystallite. In the case of the PCM with wollastonite from borogypsum, a total decline in the intensity of peaks and a shift to the larger angles are observed. The structural peculiarities of WB particles influence the formation of a crystal structure of UHMWPE.

The introduction of the binary filler results in a decrease in the intensity of amorphous and crystal phase peaks compared to UHMWPE and composites loaded only with wollastonite. It was found in a study [66] that the introduction of the organic filler into UHMWPE was followed by matrix amorphization and a decrease in crystallinity. Thus, binary filling influences the growth and form of crystallites during the structuring of the PCM, involving the deformation of crystal regions.

3.5. Tribological Properties of the Composites

Based on tribotechnical studies (Figure 12), it was found that the introduction of 1 wt.% of model wollastonite and 1 wt.% of MBT led to a 6-fold decrease in the rate of mass wear compared to the initial UHMWPE. It was observed that linear wear slowly decreased and had a “gradual character” with an increase in the content of “MBT–MW” fillers. Moreover, the friction coefficient remained at the level of the initial UHMWPE. Apart from that, a 6-fold decline in the wear rate compared to the initial UHMWPE was detected at the MW single filling. However, the friction coefficient was slightly higher than that of the composite with a binary filler.

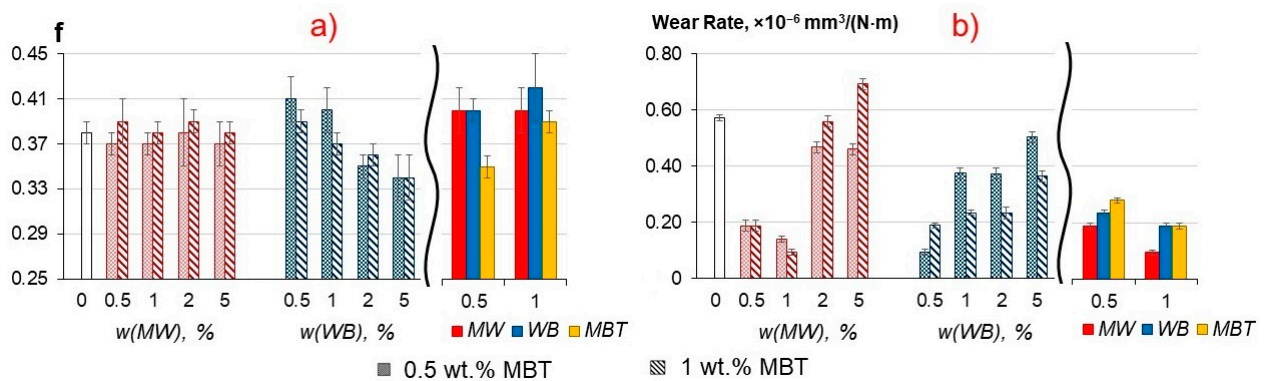


Figure 12. The dependence of the tribotechnical properties of the PCM as a function of the wollastonite content: (a) f—friction coefficient; (b) wear rate.

A 6-fold decline in the mass wear rate was noticed in the composite with 0.5 wt.% WB and 0.5 wt.% MBT, whereas single filling of WB led to a 3-fold decrease. Also, some rise of the friction coefficient was observed with the introduction of 0.5 and 1 wt.% wollastonite in UHMWPE, and then it decreased with an increase in the WB content. It is seen that a single filling with MBT did not contribute to the sufficient improvement of the tribological properties. Only a 3-fold decline in the wear rate relative to UHMWPE was observed. Thus, one may say that the introduction of two modifiers exhibits a synergetic effect since each of the components interacts differently with the matrix.

3.6. Study of the Friction Surface

To explore the regularities of changes in the material subsurface layer during friction and to explain the results obtained according to tribological tests, SEM and IR spectroscopy studies of the friction surface morphology of UHMWPE and the PCM based on the content and ratio of the fillers were conducted. Figure 13 shows the microphotographs of the friction surfaces of UHMWPE and the PCM with single filling (MBT, MW, WB).

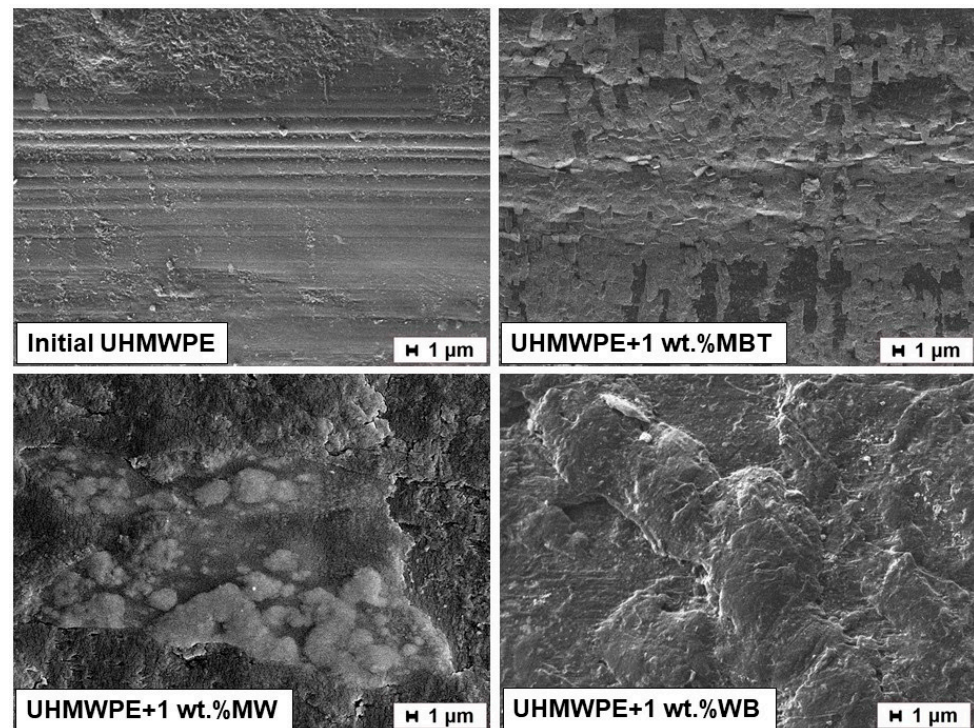


Figure 13. The morphology of the friction surface of UHMWPE and the PCM based on the filler.

The presence of the furrows oriented along the friction path resulting from the plastic deformation with the following growth of mechanical hysteresis losses in the subsurface layer of the polymer is observed on the friction surfaces of the initial UHMWPE, as seen in Figure 13. A specific morphology of the friction surface is formed due to the multiple repetitions of such processes. The composite loaded with MW is characterized by the development of tight formations, unlike the matrix, the so-called secondary structures. In the case of WB introduction, the presence of beads on the friction surface of the PCM is detected, suggesting an increase in the thermal strain at friction. Atypical morphology of the friction surface was found in the PCM consisting of MBT. The development of complex ordered structures, the so-called “clusters”, containing MBT particles, is observed.

The microphotographs of the friction surfaces of the PCM loaded with 1 wt.% MBT, depending on the wollastonite content, are presented in Figure 14.

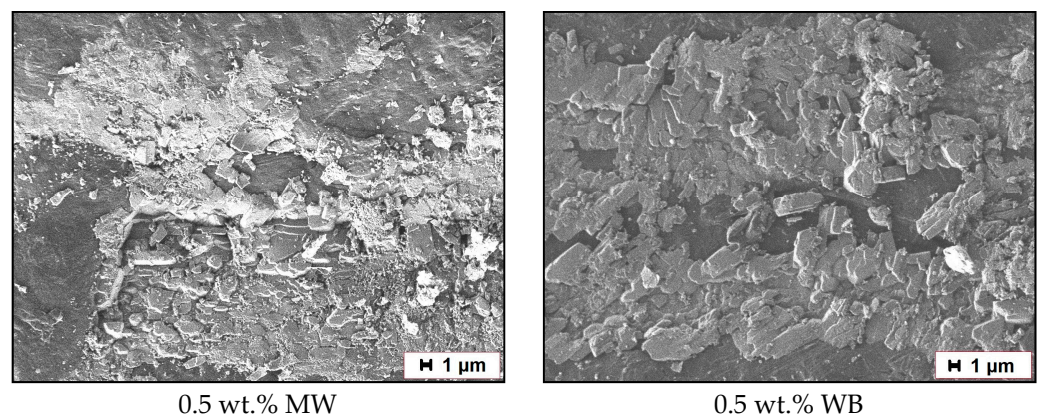


Figure 14. Cont.

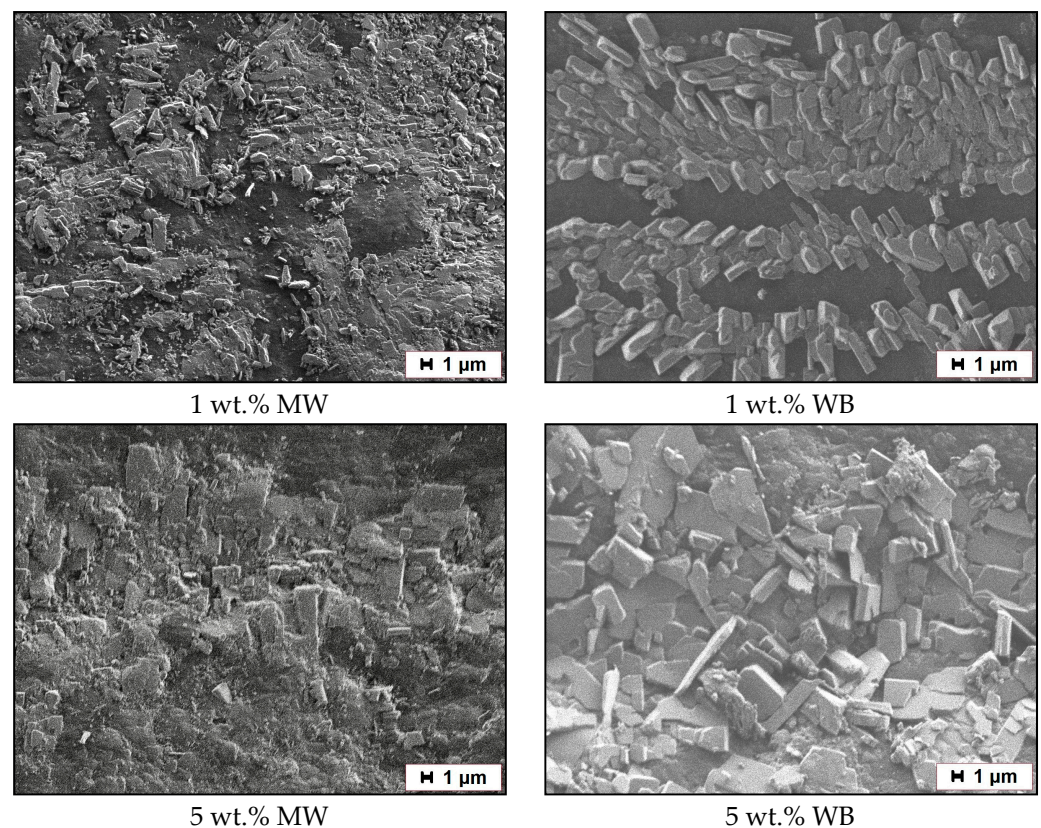


Figure 14. The microphotographs of the friction surfaces of the PCM containing 1 wt.% MBT depending on the wollastonite concentration.

A comparison of the structure of PCM friction surfaces depending on the type of wollastonite used revealed some differences: the friction surface of the composite material with WB is smoother and is characterized by a higher content of secondary structures. The secondary structure of the composite with the “MBT–MW” binary content is inhomogeneous (discontinuous). It is distinguished by local distribution on the surface (i.e., it does not cover the entire friction surface). However, oriented secondary structures develop, and wollastonite agglomerates are absent in all composites with the “MBT + wollastonite” system. The absence of matrix peeling zones and deep furrows on the friction surface indicates a decrease in the counterface abrasive effect on the material. Moreover, the absence of beads indicates the minimization of adhesive wear and destruction of material integrity, explaining the reduction by three times the mass wear rate. The wear mechanism of a binary-filled composite can be described as follows:

- In the first acts of friction, MBT (as a soft organic filler) can melt in the near-surface layer in the zone between the composites and the steel counterbody due to the increased temperature under mechanical stress. Consequently, MBT actively forms clusters on the friction surface of the composite and a transfer film on the surface of the steel counterbody [25,67]. In this case, MBT reduces the adhesion component of friction and facilitates the sliding processes of the composite relative to the surface of the steel counterbody, as if playing the role of a lubricant. The chemical aspect of MBT is described in more detail below.
- The wollastonite particles (as solid particles) reinforce the polymer matrix, thereby preventing further molding of the surface layer. Solid particles can be localized in the friction zone, resulting in a gradual enrichment of the PCM surface with the more thermostable wollastonite particles. As a result, discrete areas are formed where the filler particles absorb the external load. The reduction of stresses at frictional contact

is caused by the reduction of the actual contact area, increasing the loading capacity of the material and reducing the wear of the PCM, respectively.

The IR spectra of the friction surfaces of the PCM, depending on the used wollastonite and the MBT content, are presented in Figure 15. Absorption bands corresponding to the characteristic vibrations of UHMWPE (2914, 2847, 1462, and 719 cm^{-1}) are detected in the IR spectra. Bands at 2914, 2847, and 1462 cm^{-1} are induced by the stretching modes of the $-\text{CH}_2$ bond, and the peak at 719 cm^{-1} corresponds to the pendular oscillations of a polymeric chain.

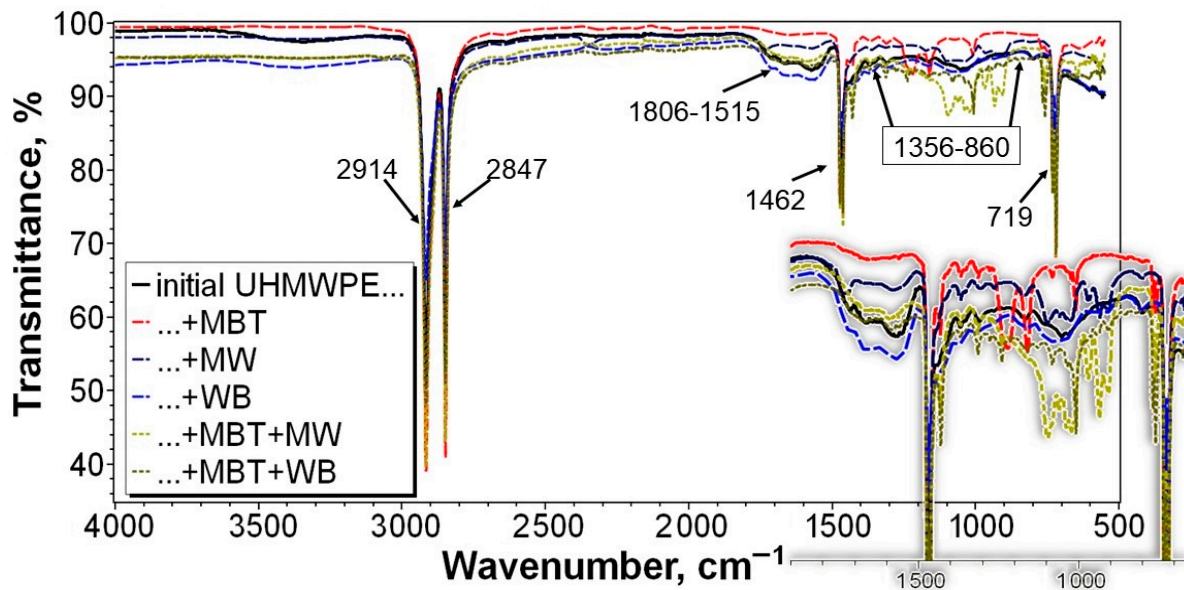


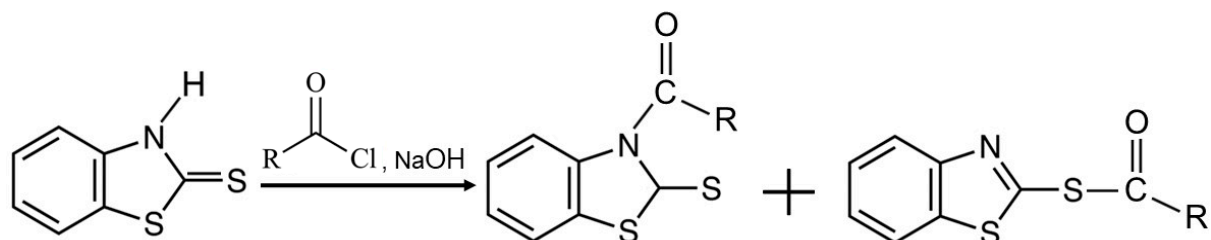
Figure 15. The IR spectra of friction surfaces of the PCM depending on the content and ratio of the filler.

It is known [21] that the presence of an absorption band at 1806–1515 cm^{-1} , evidencing the tribooxidative reaction behavior with the formation of carboxyl and carbonyl groups after friction in the IR spectra of UHMWPE-based composite materials is observed. It is seen that the composite loaded with WB is characterized by a larger intensity of the absorption band in this region. It is explained by the intensification of the tribooxidative processes due to an increase in the thermal strain in the friction zone, which leads to the formation of beads on the friction surface (Figure 13). The opposite behavior of the IR spectra is observed in the case of the composite containing MBT. It has no absorption band in this region. This suggests the formation of the protective coating on the friction surface of the PCM, which protects the material from further wear. In addition, the IR spectra consist of other absorption bands in the region of 1356–860 cm^{-1} , which can be referred to as the characteristic vibrations of both MBT and CaSiO_3 .

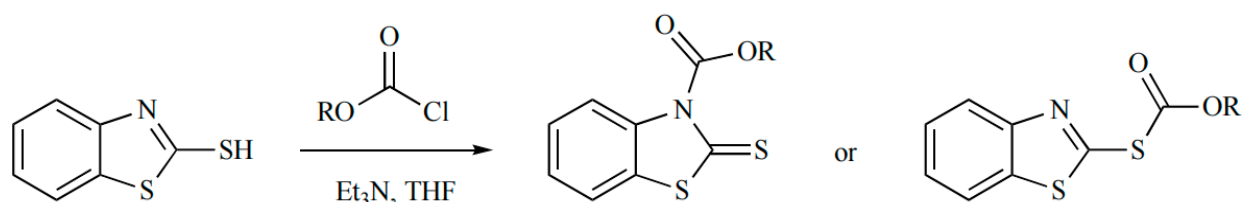
A comparison of the IR spectra of the PCM loaded with wollastonite and binary filler indicates a decline in the intensity of absorption bands in the region of 850–1100 cm^{-1} , corresponding to the vibrations of oxygen–silicon bonds. It is explained by the dispersion of filler agglomerates when introducing MBT, as shown in Figures 7–10. Structuring processes with the formation of secondary structures minimize the abrasive effect using harder filler particles (in this case, wollastonite) in the metal–polymeric contact zone.

A decrease in the intensity of the oxygen-containing groups corresponding to the carbonyl and the carboxyl groups when introducing MBT can be explained by its chemical nature. It is supposed that MBT may react with oxidative products of tribochemical reactions. Since MBT is an ambident nucleophile, the acidulation reaction can proceed through sulfur S or the nitrogen atom N(3). Harsh reaction conditions (strong bases, high temperatures, and longer reaction time) increase the yield of thermodynamically more

stable N-substituted products [68]. Thus, the interaction of MBT with chloroanhydrides and anhydride acids (Schemes 2 and 3), which yield an admixture of the N- and S-acylable products (N- acidulation prevails), was studied.

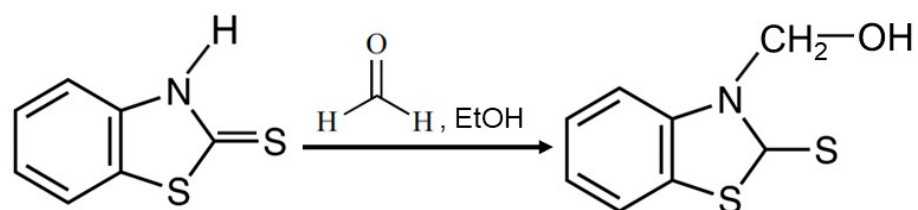


Scheme 2. The interaction of MBT with chloroanhydrides.

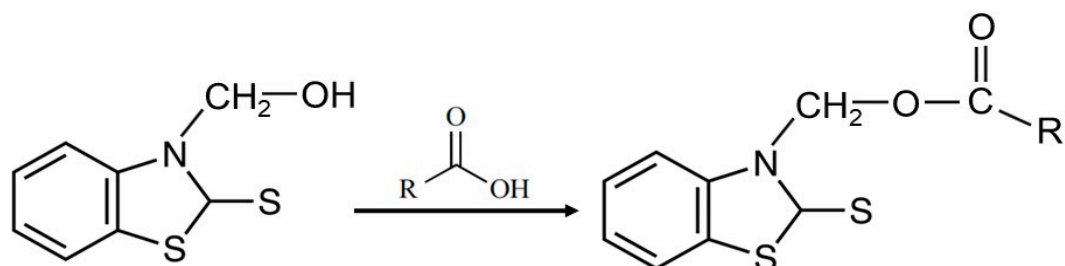


Scheme 3. The interaction of MBT with anhydride acids.

Due to the potential interaction with the carbonyl-containing oxidized products of UHMWPE, the reaction will proceed through the N atom of the thiazole ring of MBT (Scheme 4). The following interaction of the 2-sulfur-3-hydroxymethylbenzothiazol intermediate product with the carboxyl-containing oxidized products leads to the formation of the ester compounds according to reaction of the Scheme 5. The obtained ester compounds are an anti-wear additive that contributes to improved sliding of the contacting surfaces.



Scheme 4. The interaction of MBT with the carbonyl-containing oxidized products.



Scheme 5. The interaction of the 2-sulfur-3-hydroxymethylbenzothiazol with the carboxyl-containing oxidized products.

It is known [69] that MBT is a chelating agent, i.e., it can connect metal atoms of the counterface and form four-membered rings (hydrophobic complexes). In this context, the N(3) and S atoms in the thiol form are favorable reaction centers for metal atom attack. Additionally, MBT can spontaneously form a film (a self-organizing monolayer) on the counterface surface through spontaneous adsorption. Thus, a stable transferred film consisting of polymeric and reaction layers with chelate compounds may be developed on the counterface surface.

4. Conclusions

Based on the results obtained, it has been established that the binary filler consisting of an organic modifier and synthetic wollastonite is effective in the improvement of the strength–deformation properties and wear resistance of the PCM. It has been shown that the introduction of the binary complex “MBT + model wollastonite” leads to a maximum increase in tensile strength by 35%. Moreover, an increase in elongation at fracture by 22% is observed. The improvement of the strain–deformation properties of the PCM may be attributed to the improvement of the interphase interaction in the “polymer–filler” system and the matrix relaxation due to the MBT soft filler. Using XRD, it has been established that in the case of the introduction of a binary complex of modifiers to UHMWPE, the reduction in the amorphous ring and crystalline peaks on the X-ray diffraction patterns of the PCM is observed. It is caused by structure amorphization upon introducing the organic filler and steric constraints due to the interaction with the wollastonite surface.

Structural studies of the friction surfaces revealed the formation of complex ordered structures from filler crystals that protect the material from wear and adapt the material during friction. Thus, the composites with the binary complex filler are characterized by a 6-fold increase in relative wear resistance without an increase in the friction coefficient, indicating the minimization of abrasive action of the relatively hard wollastonite particles on the material and counterface.

Author Contributions: Conceptualization, S.N.D. and S.B.Y.; methodology, A.P.V. and E.K.P.; software, A.A.D. and O.O.S.; validation, I.Y.B., I.G.Z. and N.V.I.; formal analysis, A.P.V. and N.V.I.; investigation, S.N.D. and A.A.D.; resources, E.K.P. and P.S.G.; data curation, A.A.O.; writing—original draft preparation, S.N.D. and S.B.Y.; writing—review and editing, I.Y.B. and P.S.G.; visualization, S.N.D. and I.G.Z.; supervision, A.A.O.; project administration, S.B.Y.; funding acquisition, E.K.P. All authors have read and agreed to the published version of the manuscript.

Funding: Syntheses of the filler were carried out within the framework of the state assignment of the Institute of Chemistry, Far East Branch, Russian Academy of Sciences, project FWFN (0205)-2022-0002. The microstructure studies were financially within the State Assignment of the Ministry of Science and Higher Education of the Russian Federation, topic No. FZNS-2023-0003. The properties and structure of the polymer composite material were studied with the financial support of the Ministry of Education and Science of the Russian Federation No. FSRG-2021-0016.

Informed Consent Statement: Not applicable.

Data Availability Statement: The data used to support the findings of this study are available from the corresponding author upon request.

Conflicts of Interest: The authors declare that they have no known competing financial interest or personal relationships that could have appeared to influence the work reported in this paper.

References

1. Kolosov, A.E.; Sivetskii, V.I.; Kolosova, E.P.; Vanin, V.V.; Gondlyakh, A.V.; Sidorov, D.E.; Ivitskiy, I.I. Creation of Structural Polymer Composite Materials for Functional Application Using Physicochemical Modification. *Adv. Polym. Technol.* **2019**, *2019*, 1–12. [[CrossRef](#)]
2. Selyutin, G.E.; Gavrilov, Y.U.; Voskresenskaya, E.N.; Zakharov, V.A.; Nikitin, V.E.; Poluboyarov, V.A. Composite materials based on ultra-high molecular polyethylene: Properties, application prospects. *Chem. Sustain. Dev.* **2010**, *18*, 301–314.
3. Kurtz, S.M. *UHMWPE Biomaterials Handbook: Ultra High Molecular Weight Polyethylene in Total Joint Replacement and Medical Devices*, 2nd ed.; Elsevier: Amsterdam, The Netherlands; Academic Press: Boston, MA, USA, 2009; ISBN 978-0-12-374721-1.
4. Patel, K.; Chikkali, S.H.; Sivaram, S. Ultrahigh Molecular Weight Polyethylene: Catalysis, Structure, Properties, Processing and Applications. *Prog. Polym. Sci.* **2020**, *109*, 101290. [[CrossRef](#)]
5. Sobieraj, M.C.; Rinnac, C.M. Ultra High Molecular Weight Polyethylene: Mechanics, Morphology, and Clinical Behavior. *J. Mech. Behav. Biomed. Mater.* **2009**, *2*, 433–443. [[CrossRef](#)] [[PubMed](#)]
6. Hambir, S.; Jog, J.P. Sintering of Ultra High Molecular. *Bull. Mater. Sci.* **2000**, *23*, 221–226. [[CrossRef](#)]
7. Grinev, V.G.; Krashennikov, V.G.; Zabolotnov, A.S.; Ladygina, T.A.; Brevnov, P.N.; Novokshonova, L.A.; Berlin, A.A. The Effect of Filler Type on the Mechanical Properties of Composite Materials Based on Ultra-High-Molecular-Weight Polyethylene. *Polym. Sci. Ser. D* **2018**, *11*, 202–208. [[CrossRef](#)]

8. Zhang, H.; Zhao, S.; Xin, Z.; Ye, C.; Li, Z.; Xia, J.; Li, J. Mechanism of Size Effects of a Filler on the Wear Behavior of Ultrahigh Molecular Weight Polyethylene. *Chin. J. Chem. Eng.* **2020**, *28*, 1950–1963. [[CrossRef](#)]
9. Liang, W.; Xiaochun, Y.; Guangjian, H.; Yanhong, F.; Jinping, Q. Ultrasound-Assisted Melt Mixing for the Preparation of UHMWPE/OMMT Nanocomposites. *J. Thermoplast. Compos. Mater.* **2018**, *31*, 784–802. [[CrossRef](#)]
10. Yin, X.; Li, S.; He, G.; Feng, Y.; Wen, J. Preparation and Characterization of CNTs/UHMWPE Nanocomposites via a Novel Mixer under Synergy of Ultrasonic Wave and Extensional Deformation. *Ultrason. Sonochem.* **2018**, *43*, 15–22. [[CrossRef](#)]
11. Bracco, P.; Brunella, V.; Luda, M.P.; Zanetti, M.; Costa, L. Radiation-Induced Crosslinking of UHMWPE in the Presence of Co-Agents: Chemical and Mechanical Characterisation. *Polymer* **2005**, *46*, 10648–10657. [[CrossRef](#)]
12. Fu, J.; Ghali, B.W.; Lozynsky, A.J.; Oral, E.; Muratoglu, O.K. Wear Resistant UHMWPE with High Toughness by High Temperature Melting and Subsequent Radiation Cross-Linking. *Polymer* **2011**, *52*, 1155–1162. [[CrossRef](#)]
13. Kiseleva, T.Y.; Devyatkina, E.T.; Grigoreva, T.F.; Yakuta, E.V.; Lazareva, E.V.; Vosmerikov, S.V.; Zholudev, S.I.; Ivanenko, I.P.; Markov, G.P.; Sangaa, D.; et al. Mechanosynthesized Composite Materials Based on Ultrahigh Molecular Weight Polyethylene Modified with Magnesium Ferrite Particles. *Inorg. Mater. Appl. Res.* **2021**, *12*, 740–749. [[CrossRef](#)]
14. Panin, V.E.; Panin, S.V.; Kornienko, L.A.; Vannasri, S.; Ivanova, L.R.; Shil'ko, S.V. Effect of Mechanical Activation of Ultra-High-Molecular-Weight Polyethylene on Its Mechanical and Tribotechnology Properties. *J. Frict. Wear* **2010**, *31*, 121–127. [[CrossRef](#)]
15. Pak, S.Y.; Kim, H.M.; Kim, S.Y.; Youn, J.R. Synergistic Improvement of Thermal Conductivity of Thermoplastic Composites with Mixed Boron Nitride and Multi-Walled Carbon Nanotube Fillers. *Carbon* **2012**, *50*, 4830–4838. [[CrossRef](#)]
16. Papynov, E.K.; Mayorov, V.Y.; Portnyagin, A.S.; Shichalin, O.O.; Kobyljakov, S.P.; Kaidalova, T.A.; Nepomnyashiy, A.V.; Sokol'nitskaya, T.A.; Zub, Y.L.; Avramenko, V.A. Application of Carbonaceous Template for Porous Structure Control of Ceramic Composites Based on Synthetic Wollastonite Obtained via Spark Plasma Sintering. *Ceram. Int.* **2015**, *41*, 1171–1176. [[CrossRef](#)]
17. Papynov, E.K.; Shichalin, O.O.; Apanasevich, V.I.; Portnyagin, A.S.; Yu, M.V.; Yu, B.I.; Merkulov, E.B.; Kaidalova, T.A.; Modin, E.B.; Afonin, I.S.; et al. Sol-Gel (Template) Synthesis of Osteoplastic CaSiO₃/HAp Powder Biocomposite: “In Vitro” and “in Vivo” Biocompatibility Assessment. *Powder Technol.* **2020**, *367*, 762–773. [[CrossRef](#)]
18. Papynov, E.K.; Shichalin, O.O.; Apanasevich, V.I.; Afonin, I.S.; Evdokimov, I.O.; Mayorov, V.Y.; Portnyagin, A.S.; Agafonova, I.G.; Skurikhina, Y.E.; Medkov, M.A. Synthetic CaSiO₃ Sol-Gel Powder and SPS Ceramic Derivatives: “In Vivo” Toxicity Assessment. *Prog. Nat. Sci. Mater. Int.* **2019**, *29*, 569–575. [[CrossRef](#)]
19. Tong, J.; Ma, Y.; Jiang, M. Effects of the Wollastonite Fiber Modification on the Sliding Wear Behavior of the UHMWPE Composites. *Wear* **2003**, *255*, 734–741. [[CrossRef](#)]
20. Panin, S.V.; Huang, Q.; Alexenko, V.O.; Buslovich, D.G.; Kornienko, L.A.; Berto, F.; Bochkareva, S.A.; Panov, I.L.; Ryabova, N.V. Design of Wear-Resistant UHMWPE-Based Composites Loaded with Wollastonite Microfibers Treated with Various Silane Coupling Agents. *Appl. Sci.* **2020**, *10*, 4511. [[CrossRef](#)]
21. Danilova, S.N.; Yarusova, S.B.; Kulchin, Y.N.; Zhevtun, I.G.; Buravlev, I.Y.; Okhlopko, A.A.; Gordienko, P.S.; Subbotin, E.P. UHMWPE/CaSiO₃ Nanocomposite: Mechanical and Tribological Properties. *Polymers* **2021**, *13*, 570. [[CrossRef](#)]
22. Danilova, S.N.; Yarusova, S.B.; Lazareva, N.N.; Buravlev, I.Y.; Shichalin, O.O.; Papynov, E.K.; Zhevtun, I.G.; Gordienko, P.S.; Okhlopko, A.A. A Study of the Wear Mechanism of Composites Modified with Silicate Filler. *Ceramics* **2022**, *5*, 731–747. [[CrossRef](#)]
23. Mahfoudh, A.; Cloutier, A.; Rodrigue, D. Characterization of UHMWPE/Wood Composites Produced via Dry-Blending and Compression Molding. *Polym Compos* **2013**, *34*, 510–516. [[CrossRef](#)]
24. Duraccio, D.; Arrigo, R.; Strongone, V.; Capra, P.P.; Malucelli, G. Rheological, Mechanical, Thermal and Electrical Properties of UHMWPE/CNC Composites. *Cellulose* **2021**, *28*, 10953–10967. [[CrossRef](#)]
25. Panin, S.V.; Kornienko, L.A.; Nguen Suan, T.; Ivanova, L.R.; Korchagin, M.A.; Shil'ko, S.V.; Pleskachevskii, Y.M. Wear Resistance of Composites Based on Hybrid UHMWPE–PTFE Matrix: Mechanical and Tribotechnical Properties of the Matrix. *J. Frict. Wear* **2015**, *36*, 249–256. [[CrossRef](#)]
26. Massaccesi, L.; Ragone, V.; Papini, N.; Goi, G.; Corsi Romanelli, M.M.; Galliera, E. Effects of Vitamin E-Stabilized Ultra High Molecular Weight Polyethylene on Oxidative Stress Response and Osteoimmunological Response in Human Osteoblast. *Front. Endocrinol.* **2019**, *10*, 203. [[CrossRef](#)]
27. GOST 739-74; 2-Mercaptobenzothiazole. Specifications, Standards Publishing House: Moscow, Russia, 2000; 11p.
28. ASTM A. D3039/D3039M-14; Tensile Properties of Polymer Matrix Composite Materials, Annu. Book ASTM Stand. ASTM International: West Conshohocken, PA, USA, 2014; p. 13.
29. Chesick, J.P.; Donohue, J. The Molecular and Crystal Structure of 2-Mercaptobenzothiazole. *Acta Crystallogr. B Struct. Sci.* **1971**, *27*, 1441–1444. [[CrossRef](#)]
30. Rai, A.K.; Singh, R.; Singh, K.N.; Singh, V.B. FTIR, Raman Spectra and Ab Initio Calculations of 2-Mercaptobenzothiazole. *Spectrochim. Acta Part A Mol. Biomol. Spectrosc.* **2006**, *63*, 483–490. [[CrossRef](#)]
31. Chattaraj, P.K.; Sarkar, U.; Roy, D.R. Electrophilicity Index. *Chem. Rev.* **2006**, *106*, 2065–2091. [[CrossRef](#)]
32. Obot, I.B.; Gasem, Z.M.; Umoren, S.A. Understanding the mechanism of 2-mercaptobenzimidazole adsorption on Fe (110), Cu (111) and Al (111) surfaces: DFT and molecular dynamics simulations approaches. *Int. J. Electrochem. Sci.* **2014**, *9*, 2367–2378. [[CrossRef](#)]

33. Vernack, E.; Costa, D.; Tingaut, P.; Marcus, P. DFT Studies of 2-Mercaptobenzothiazole and 2-Mercaptobenzimidazole as Corrosion Inhibitors for Copper. *Corros. Sci.* **2020**, *174*, 108840. [[CrossRef](#)]
34. Huang, W.; Dong, J.; Li, F.; Chen, B. The Performance and Antiwear Mechanism of (2-Sulfurone-Benzothiazole)-3-Methyl Esters as Additives in Synthetic Lubricant. *Tribol. Int.* **2000**, *33*, 553–557. [[CrossRef](#)]
35. Feng, Y.; Chen, S.; Zhang, H.; Li, P.; Wu, L.; Guo, W. Characterization of Iron Surface Modified by 2-Mercaptobenzothiazole Self-Assembled Monolayers. *Appl. Surf. Sci.* **2006**, *253*, 2812–2819. [[CrossRef](#)]
36. Kress, K.E. Spectrophotometric Analysis of Accelerator-Rubber Mixtures. *Anal. Chem.* **1951**, *23*, 313–322. [[CrossRef](#)]
37. Alam, M.N.; Debnath, S.C.; Boondamnoen, O.; Kumar, K.N.; Kim, J.H.; Choi, J. Synergistic Combination of 2-Mercaptobenzothiazole (MBT) and Nitrosoamine-Safe Thiuram Disulfide as Advanced Rubber Vulcanizing Accelerators. *J. Elastomers Plast.* **2022**, *54*, 1061–1077. [[CrossRef](#)]
38. Liu, Y.; Wang, H.; Guo, X.; Yi, M.; Wan, L.; Liao, S.; Wang, Z.; Fang, L. Xanthate-Modified NanoTiO₂ as a Novel Vulcanization Accelerator Enhancing Mechanical and Antibacterial Properties of Natural Rubber. *Nanotechnol. Rev.* **2021**, *10*, 478–487. [[CrossRef](#)]
39. Ilichev, V.A.; Silantyeva, L.I.; Yablonskiy, A.N.; Andreev, B.A.; Romyantsev, R.V.; Fukin, G.K.; Bochkarev, M.N. Synthesis, Structure and Long-Lived NIR Luminescence of Lanthanide Ate Complexes with Perfluorinated 2-Mercaptobenzothiazole. *Dalton Trans.* **2019**, *48*, 1060–1066. [[CrossRef](#)]
40. Form, G.R.; Raper, E.S.; Downie, T.C. The Crystal and Molecular Structure of 2-Mercaptobenzimidazole. *Acta Crystallogr. B Struct. Sci.* **1976**, *32*, 345–348. [[CrossRef](#)]
41. Rogozhin, A.F.; Ilichev, V.A.; Fagin, A.A.; Romyantsev, R.V.; Fukin, G.K.; Yablonskiy, A.N.; Andreev, B.A.; Bochkarev, M.N. Novel Ditopic 2-Mercaptothiazoles and Their Sodium Salts: Synthesis, Structural Diversity and Luminescence. *New J. Chem.* **2022**, *46*, 13987–13995. [[CrossRef](#)]
42. Flakus, H.T.; Miros, A.; Jones, P.G. Polarization IR Spectra of Model Crystals Containing Cyclic N–H...S Bonded Dimers: 2-Mercaptothiazoline and 2-Mercapto-1-Methylimidazole. *Spectrochim. Acta Part A Mol. Biomol. Spectrosc.* **2002**, *58*, 225–237. [[CrossRef](#)]
43. Silva, A.L.R.; Ribeiro da Silva, M.D.M.C. Energetic, Structural and Tautomeric Analysis of 2-Mercaptobenzimidazole: An Experimental and Computational Approach. *J. Therm. Anal. Calorim.* **2017**, *129*, 1679–1688. [[CrossRef](#)]
44. Mohamed, T.A.; Mustafa, A.M.; Zoghaib, W.M.; Afifi, M.S.; Farag, R.S.; Badr, Y. Reinvestigation of Benzothiazoline-2-Thione and 2-Mercaptobenzothiazole Tautomers: Conformational Stability, Barriers to Internal Rotation and DFT Calculations. *J. Mol. Struct. THEOCHEM* **2008**, *868*, 27–36. [[CrossRef](#)]
45. Radha, A. Crystal and Molecular Structure of 2-Mercaptobenzothiazole—A Redetermination. *Z. Für Krist. Cryst. Mater.* **1985**, *171*, 225–228. [[CrossRef](#)]
46. Böhlig, H.; Ackermann, M.; Billes, F.; Kudra, M. Vibrational Analysis of Benzothiazoline-2-Thione. *Spectrochim. Acta Part A Mol. Biomol. Spectrosc.* **1999**, *55*, 2635–2646. [[CrossRef](#)]
47. Okhlopkova, T.A.; Borisova, R.V.; Nikiforov, L.A.; Spiridonov, A.M.; Sharin, P.P.; Okhlopkova, A.A. Technology of Liquid-Phase Compounding of Ultra-High-Molecular-Weight Polyethylene with Nanoparticles of Inorganic Compounds under the Action of Ultrasonic Vibrations. *Russ. J. Appl. Chem.* **2016**, *89*, 1469–1476. [[CrossRef](#)]
48. Okhlopkova, T.A.; Borisova, R.V.; Nikiforov, L.A.; Spiridonov, A.M.; Okhlopkova, A.A.; Jeong, D.-Y.; Cho, J.-H. Supramolecular Structure and Mechanical Characteristics of Ultrahigh-Molecular-Weight Polyethylene-Inorganic Nanoparticle Nanocomposites: UHMWPE-Inorganic Nanoparticle Composites. *Bull. Korean Chem. Soc.* **2016**, *37*, 439–444. [[CrossRef](#)]
49. Kapitonova, I.; Lazareva, N.; Tarasova, P.; Okhlopkova, A.; Laukkanen, S.; Mukhin, V. Morphology Analysis of Friction Surfaces of Composites Based on PTFE and Layered Silicates. *Polymers* **2022**, *14*, 4658. [[CrossRef](#)]
50. Berladir, K.; Zhyhylii, D.; Gaponova, O.; Krmela, J.; Krmelová, V.; Artyukhov, A. Modeling of Polymer Composite Materials Chaotically Reinforced with Spherical and Cylindrical Inclusions. *Polymers* **2022**, *14*, 2087. [[CrossRef](#)]
51. Mostovoy, A.; Bekeshev, A.; Tastanova, L.; Akhmetova, M.; Bredihin, P.; Kadykova, Y. The Effect of Dispersed Filler on Mechanical and Physicochemical Properties of Polymer Composites. *Polym. Polym. Compos.* **2021**, *29*, 583–590. [[CrossRef](#)]
52. Sarokin, V.; Avdeychik, S.; Struk, V.; Antonov, A. Activation of components functional polymer materials according to energy technologies. In Proceedings of the 21st International Scientific Conference, Kaunas, Lithuania, 12–13 May 2016; pp. 241–244.
53. Costa, P.; Maceiras, A.; San Sebastián, M.; García-Astrain, C.; Vilas, J.L.; Lanceros-Mendez, S. On the Use of Surfactants for Improving Nanofiller Dispersion and Piezoresistive Response in Stretchable Polymer Composites. *J. Mater. Chem. C* **2018**, *6*, 10580–10588. [[CrossRef](#)]
54. Cheng, C.; Shi, W.-H.; Teng, T.-P.; Yang, C.-R. Evaluation of Surfactants on Graphene Dispersion and Thermal Performance for Heat Dissipation Coating. *Polymers* **2022**, *14*, 952. [[CrossRef](#)]
55. Atif, R.; Inam, F. Reasons and Remedies for the Agglomeration of Multilayered Graphene and Carbon Nanotubes in Polymers. *Beilstein J. Nanotechnol.* **2016**, *7*, 1174–1196. [[CrossRef](#)] [[PubMed](#)]
56. Yousef, S.; Visco, A.; Galtieri, G.; Nocita, D.; Espro, C. Wear Behaviour of UHMWPE Reinforced by Carbon Nanofiller and Paraffin Oil for Joint Replacement. *Mater. Sci. Eng. C* **2017**, *73*, 234–244. [[CrossRef](#)] [[PubMed](#)]
57. Visco, A.; Yousef, S.; Scolaro, C.; Espro, C.; Cristani, M. Tribological Behavior of Nanocomposites Based on UHMWPE Aged in Simulated Synovial Fluid. *Polymers* **2018**, *10*, 1291. [[CrossRef](#)] [[PubMed](#)]

58. Catauro, M.; Scolaro, C.; Dal Poggetto, G.; Pacifico, S.; Visco, A. Wear Resistant Nanocomposites Based on Biomedical Grade UHMWPE Paraffin Oil and Carbon Nano-Filler: Preliminary Biocompatibility and Antibacterial Activity Investigation. *Polymers* **2020**, *12*, 978. [[CrossRef](#)] [[PubMed](#)]
59. Parpaite, T.; Otazaghine, B.; Caro, A.S.; Taguet, A.; Sonnier, R.; Lopez-Cuesta, J.M. Janus Hybrid Silica/Polymer Nanoparticles as Effective Compatibilizing Agents for Polystyrene/Polyamide-6 Melted Blends. *Polymer* **2016**, *90*, 34–44. [[CrossRef](#)]
60. Jiang, J.; Cao, J.; Wang, W.; Shen, H. Preparation of a Synergistically Stabilized Oil-in-Water Paraffin Pickering Emulsion for Potential Application in Wood Treatment. *Holzforschung* **2018**, *72*, 489–497. [[CrossRef](#)]
61. Jiang, J.; Mei, C.; Pan, M.; Cao, J. How Does Pickering Emulsion Pre-Treatment Influence the Properties of Wood Flour and Its Composites with High-Density Polyethylene? *Polymers* **2019**, *11*, 1115. [[CrossRef](#)]
62. Vignati, E.; Piazza, R.; Lockhart, T.P. Pickering Emulsions: Interfacial Tension, Colloidal Layer Morphology, and Trapped-Particle Motion. *Langmuir* **2003**, *19*, 6650–6656. [[CrossRef](#)]
63. Kurkin, T.S.; Ozerin, A.N.; Kechek'yan, A.S.; Gritsenko, O.T.; Ozerina, L.A.; Alkhanishvili, G.G.; Sushchev, V.G.; Dolmatov, V.Y. The Structure and Properties of Polymer Composite Fibers Based on Poly(Vinyl Alcohol) and Nanodiamond of Detonation Synthesis. *Nanotechnol. Russ.* **2010**, *5*, 340–351. [[CrossRef](#)]
64. Taguet, A.; Cassagnau, P.; Lopez-Cuesta, J.-M. Structuration, Selective Dispersion and Compatibilizing Effect of (Nano)Fillers in Polymer Blends. *Prog. Polym. Sci.* **2014**, *39*, 1526–1563. [[CrossRef](#)]
65. Hu, X.-P.; Hsieh, Y.-L. Crystallite Sizes and Lattice Distortions of Gel-Spun Ultra-High Molecular Weight Polyethylene Fibers. *Polym. J.* **1998**, *30*, 771–774. [[CrossRef](#)]
66. Danilova, S.N.; Dyakonov, A.A.; Vasilev, A.P.; Okhlopkova, A.A.; Tuisov, A.G.; Kychkin, A.K.; Kychkin, A.A. Effect of Borpolymer on Mechanical and Structural Parameters of Ultra-High Molecular Weight Polyethylene. *Nanomaterials* **2021**, *11*, 3398. [[CrossRef](#)] [[PubMed](#)]
67. Kar, M.K.; Bahadur, S. Micromechanism of Wear at Polymer-Metal Sliding Interface. *Wear* **1978**, *46*, 189–202. [[CrossRef](#)]
68. Romani, S.; Moroder, L.; Bovermann, G.; Wunsch, E. On the Use of Five-Membered Heterocycles in Peptide Chemistry. *Synthesis* **1985**, *1985*, 738–742. [[CrossRef](#)]
69. Yekeler, H.; Yekeler, M. Predicting the Efficiencies of 2-Mercaptobenzothiazole Collectors Used as Chelating Agents in Flotation Processes: A Density-Functional Study. *J. Mol. Model.* **2006**, *12*, 763–768. [[CrossRef](#)] [[PubMed](#)]

Disclaimer/Publisher's Note: The statements, opinions and data contained in all publications are solely those of the individual author(s) and contributor(s) and not of MDPI and/or the editor(s). MDPI and/or the editor(s) disclaim responsibility for any injury to people or property resulting from any ideas, methods, instructions or products referred to in the content.